MRS Advances © 2016 Materials Research Society
DOI: 10.1557/adv.2016.393

Microring Resonators and Silicon Photonics

Fernando Ramiro-Manzano[1], Stefano Biasi[1], Martino Bernard[2], Mattia Mancinelli[1], Tatevik Chalyan[1], Fabio Turri[1], Mher Ghulinyan[2], Massimo Borghi[1], Alina Samusenko[2], Davide Gandolfi[1], Romain Guider[1], Alessandro Trenti[1], Pierre-É. Larré[3], Laura Pasquardini[4,*], Nikola Prltjaga[1,†], Santanu Mana[1,‡], Iacopo Carusotto[3], Georg Pucker[2], and Lorenzo Pavesi[1].

[1] Nanoscience Laboratory, Department of Physics, University of Trento,
Via Sommarive 14, I-38123 Trento, Italy.
[2] Centre for Materials and Microsystems, Fondazione Bruno Kessler,
Via Santa Croce, 77, I-38123 Trento, Italy.
[3] INO-CNR BEC Center and Department of Physics, University of Trento,
Via Sommarive 14, I-38123 Trento, Italy.
[4] LaBSSAH, Fondazione Bruno Kessler,
Via Santa Croce, 77, I-38123 Trento, Italy.

* Present address: Department of Industrial Engineering, University of Trento,
Via Sommarive 9, I-38123 Trento, Italy.
† Present address: Department of Physics and Astronomy, University of Sheffield,
Sheffield S3 7RH, United Kingdom.
‡ Present address: Department of Physics and Meteorology, Indian Institute of Technology, Kharagpur, 721302, India.

ABSTRACT

Silicon Photonics is the technological to face the future challenges in data communications and processing. This technology follows the same paradigm as the technological revolution of the integrated circuit industry, that is, the miniaturization and the standardization. One of the most important building blocks in Silicon Photonics is the microresonator, a circular optical cavity, which enables many different passive and active optical functions. Here, we will describe the new physics of the intermodal coupling, which occurs when multi radial mode resonators are coupled to waveguides, and of the optical chaos, which develops in coupled sequence of resonators. In addition, an application of resonators in the label-free biosensing will be discussed.

INTRODUCTION

Electronic and communication technologies are changing our lives. Global social interactions, internet, high-yield computer-assisted workflow, rapid diagnosis and personalized cures are few basic examples of new frontiers opened by this technological progress. These advances have generated a growing demand of improvement in communication bandwidth and in computation speed for both consumer products and infrastructure installations.
In the last decade, the rapid diffusion of cloud computing for data storage, entertainment and social media, significantly contributed to the increasing demand of bandwidth for data

transmission and computing [1,2,3,4]. One of the most representative examples is the continuous increase of data traffic in North America that has risen by one order of magnitude in 9 years (from 10^3 PB/month in 2007 to 10^4 PB/month in 2016) with an additional predicted rise to another order of magnitude in 2020 [5]. The evolution of the optical fiber communication link has enabled this exponential growth of data traffic. Since their introduction in the early 1960s, when signal attenuation exceeded 1000 $dBkm^{-1}$, propagation losses have been constantly decreased to less than 0.2 $dBkm^{-1}$ at a wavelength of 1.55 μm [6]. Since the early 1970s, the system capacity, i.e., the maximum amount of bits sent in one second in a single fiber, has improved by five orders of magnitude [7]. This has been possible by data multiplexing in different wavelengths [8], the reduction of the modal birefringence and the efficient tailor of the chromatic dispersion in fibers.

The transceivers have followed a similar progress. Very Large Scale Integration (VLSI), which is the continuous size reduction of the electronic and optical components, imply higher component density and enhanced computing capabilities. This concept is well exemplified by the famous Moore's law, introduced for the first time in 1965, and which states that the number of functions per microelectronic chip would double every two years [9]. Miniaturization has been possible by the huge investments of the semiconductor industry in Integrated Circuit (IC) facilities, which in turn was motivated by the increasingly demands of the market. VLSI has been pursued to reduce the device cost by economy of scale. A synergy between different industries declared the success of VLSI: both equipment manufactures and semiconductor producers worked together to reach this common goal [10].

During these developments, a severe power problem emerged which questioned the possibility to follow the Moore's law [11]. The high electrical power density generated in a single heavily integrated chip limits the operation frequency of a single processing unit to few GHz. A further increase in frequency will cause the failure of the component due to thermal issue. Therefore, to increase the computing power the only solution was to introduce multiple core processors. However, this in turn caused the rise of the so-called interconnect bottleneck: many cores have to exchange data at a very high pace that settles the ultimate computing speed.

One of the most powerful technology to overcome the interconnect bottleneck is Silicon Photonics [12, 13, 14]. Silicon Photonics factorize the successes of microelectronics by using standard silicon processing and of optical communication by using photons to code the information. In this way, one can merge on the same chip electronic and photonic functionalities, i.e. computation and communication. Integrated photonic circuits are fabricated by using the well-developed infrastructures of Complementary Metal Oxide Semiconductor (CMOS) technology, which allows large scale integration in a cost-effective and monolithic manner.

At first, the basic discrete components have been demonstrated. These included both passive devices - such as waveguides, splitters, grating couplers and interferometers - and active ones - like modulators, hybrid lasers and photodetectors. Then, these building blocks have been connected together, and assembled in integrated circuits to realize more complex functions. As a last step, photonic devices have been integrated with electronic ones to realize optoelectronic circuits. The latter has been done by using only a limited number of materials (Silicon, Silicon Oxide, and other group IV compounds and metals) and the CMOS processing technology [15]. Silicon Photonics is not limited to data and telecom applications. The versatility of the building blocks has been exploited for applications in security, medical diagnostics [16], lab-on-chip [17,18], spectrometer-on-a-chip [19], environmental monitoring [20], neural networks [21,22].

In this paper, we will focus on the most used building block in Si-photonics, the micro-resonator. We will review our research activity about the coupling of micro-resonators with a bus waveguide and with other micro-resonators. In particular, we will report on a non-conventional coupling method, the vertical coupling between a resonator and a waveguide, and on a non-linear effect obtained through the coupling of several resonators in a chain, and, finally, on an application of micro-resonators in label-free biosensing.

EXPERIMENTS

The devices used in our experiments were made by Si-based materials. Table I details the fabrication parameters while Table II summaries the characterization procedure.

Table I: Fabrication details.

	Vertical-Coupling	**Coupled Cavities**	**Biosensors**
Resonator	Microdisk	microring	racetrack
Coupling method waveguide/cavity	Vertical	in-plane	in-plane
Cavity material	Si_xN_y	Si	SiON (n=1.6)*
Waveguide material	SiON	Si	SiON (n=1.6)*
Number of cavities	1	8 (Coupled)	4 (multiplexed)
Cavity Radius	20 μm	3.5 μm	50 μm
Cavity waveguide height	350 nm	220 nm	350 nm
Bus waveguide height	250 nm	220 nm	350 nm
Cavity waveguide width	-	500 nm	1 μm
Bus waveguide width	400 nm	500 nm	900 nm
Gap waveguide/cavity	700 nm (vertical)	300 nm (horizontal)	400 nm (horizontal)
Coupled cavity gap	-	22 μm	-
BOX (buried oxide)	3 μm	2 μm	4 μm
Additional details	[23]	[24]	[25]

(*) The refractive index (n) of the SiON was chosen to be 1.6

Table II: Characterization procedure

	Vertical-Coupling	**Coupled Cavities**	**Biosensors**
Wavelength	Around 1550nm	Around 1550nm	Around 780nm
Laser	External cavity	External Cavity	VCSEL
Light-guiding	Free Space	Fiber	Fiber
Amplification	-	EDFA	-
Detector	Large area Ge	Fast-Ge	Large area Si
Alignment system	Piezo-positioner	Piezo-positioner	Micro-motor
Insertion system	Objectives	Lensed-fibers	Lensed-fibers
Peculiarity	Mach-Zehnder interferometer (Phase measurement)	Oscilloscope Modulator	Four detectors
Additional details		[24]	[25]

DISCUSSION

Micro-resonators and coupling regimes

The micro-resonators are interesting because of their small mode volume, very high power density and narrow spectral linewidth. This makes them a unique tool for a wide range of applications spanning from nonlinear optics and quantum electrodynamics to biosensig [26]. One of the most employed integrated cavities is the whispering gallery mode (WGM) resonators, which is based on a circular symmetry. The light propagates around the periphery of the cavity performing round trips and interfering constructively. Light is inserted and extracted from the resonator by coupling to bus waveguides. This coupling determines the main properties of the system.

The transmission (T) and phase (θ) at the output of the waveguide can be described by the following relations [27,28]:

$$T = \left|\frac{E_{t1}}{E_{i1}}\right| = \frac{\alpha^2 - 2k\alpha\cos(\varphi) + k^2}{1 - -2k\alpha\cos(\varphi) + k^2\alpha^2} \qquad \theta = \arg\left(\frac{E_{t1}}{E_{i1}}\right)$$

where E_{ab} represents the normalized mode amplitudes entering (a=i) and exiting (a=t) the waveguide (b=1) or the resonator (b=2, see figure 1); φ is the round-trip phase shift $\varphi = 2\pi n_{eff} L/\lambda$, where n_{eff}, L and λ are the effective index, the perimeter and wavelength, respectively; α represents the loss coefficient of the ring ($E_{i2} = \alpha E_{i2} e^{i\varphi}$); and k and t are the coupling parameters and transmission parameters, respectively ($t^2+k^2=1$, assuming a lossless coupling).

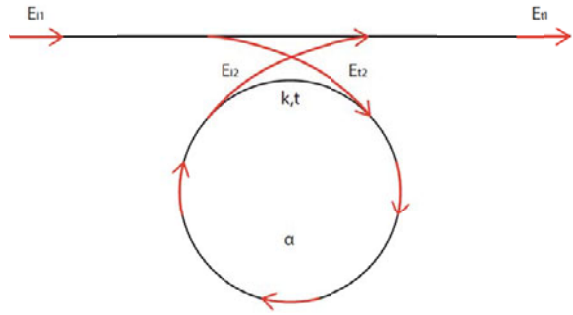

Figure 1. Sketch of a unidirectional coupling between a single ring resonator and a waveguide. E_{ab} represents the normalized mode amplitudes entering (a=i) and exiting (a=t) the waveguide (b=1) and the resonator (b=2); k and t are the coupling parameters; and α is the ring power loss coefficient. The arrows indicate the propagating direction.

On resonance (i.e. $\varphi = 2\pi m$, where m is an integer number), when the intrinsic losses are equal to the coupling losses (k = α) the coupling regime is named critically coupling, while for k>α and k<α it is named under-coupled and over-coupled regime, respectively. While the critical coupling regime and its parameters (k and α) are unequivocally determined by the transmission spectrum, since in this case it is characterized by a vanishing transmission on resonance (see figure 2a), the other regimes present similar transmittance response showing a net signal transmission (see figure 2a). As a result, neither the coupling regime nor parameters could be determined by only transmission measurements of a single resonance. However, as figure 2b shows, the under- and over-coupling regimes present different phase behavior. In particular, when the system is under-coupled, the phase shift cancels on resonance while in over-coupling a π-shift is induced on resonance resulting in a 2π total shift.

Figure 2c-d shows the transmittance and phase measured on a resonant mode not in the critical coupling regime. In fact, the on-resonance zero-phase shift (figure 2d) illustrates the under-coupling regime. In order to fit the experimental data, we have extracted a radius of the circulating mode (R = 24920 nm) similar to the nominal one (25000 nm) by fixing the resonant spectral position in a simple FEM (Finite Element Method) simulation. The parameters extracted from the data fitting are: k = 0.995± 0.002, α = 0.983 ± 0.001 and the effective refractive index, n_{eff} =1.604 ± 0.003. Consequently, the method that consists in a simultaneous fit of the transmission and of the phase permits to extract the coupling parameters, and thus to asses the coupling regime.

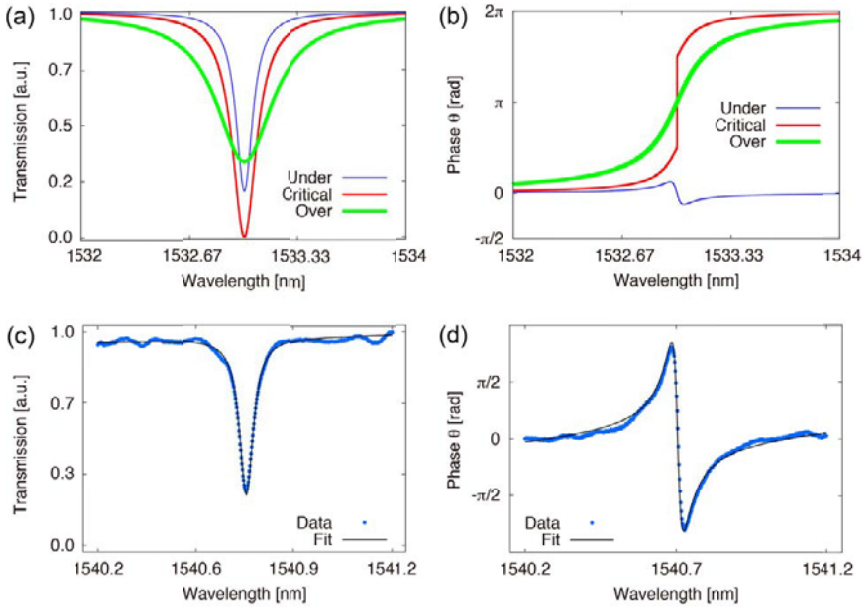

Figure 2. Computed transmission (a) and phase (b) spectra around a resonance of a micro-ring resonator. The curves correspond to different coupling regimes obtained by fixing the amplitude transmission factor ($\alpha \approx 0.97$) and varying the coupling parameters (k). (c) and (d): measured (broad data points) and simulated (narrow line) transmission and phase spectra of a resonance of a micro-ring resonator (Table I).

Vertical Coupling and Intermodal Coupling

The micro-resonator and the waveguide are usually on the same plane. This permits to define accurately the gap between both devices through the same lithographic mask. Operation which is crucial because it determines the coupling regime. Another alternative scheme consists on burying the waveguide under the resonator. In this way, the gap could be controlled at the nanometer level by deposition and etching. In addition to relax the constraints on the lithography, this permits to use different materials (such as III-V and Si) for the resonator and the waveguide. An issue is to keep a perfect planarity in the deposited layers, during the different process steps. Chemical-mechanical planarization could be used. We developed an alternative process based on boron-phosphorous-silicate-glass (BPSG) deposition, thermal reflow and etching [29,30]. We validated the method by fabricating Silicon Nanocrystals (Si-nc) resonators vertically coupled to SiON waveguides [31]. Thermally induced optical bistability was measured where the non-linear phenomenon is produced only in the absorbing media of the resonator, while the contribution to the nonlinear measurements of the bus waveguide, which is made of high transparent material, is negligible.

This coupling scheme not only allows to employ several materials but also increase the degrees of freedom. In fact, the coupling is now determined by two geometrical distances: the vertical gap tunes the coupling coefficients, while the bus waveguide-to-resonator relative horizontal position selects the radial mode family to which the light is coupled [32]. This allows coupling of bus waveguides with high quality factor wedge-resonators, where the modes are retracted from the external rim [33].

Moreover, the interaction of the micro-resonators and the waveguide is changed from a single point interaction (characteristic for the in-plane configuration) to an extended coupling region, called flat zone, which is typical of the vertical coupling [34]. In this last situation, the coupling geometry could be approximated by a directional coupler where the oscillatory coupling as a function as the vertical gap [34] or wavelength [35] causes the presence of the critical, over- and under- coupling regimes in the same micro-resonator.

This peculiarity of the vertical coupling could be employed to realize in a photonic system a situation which is very similar to Lamb-shift of hydrogen states the in atomic physics. The intermodal reactive coupling between several radial mode families of a single micro-resonator mediated by the bus waveguide gives rise to Fano-lineshapes in the transmission spectrum and to a net resonance shift due to the reactive nature of the established coupling [36]. We have formulated a model for describing this phenomenon, defined by the following equations [36]:

$$t(\omega_{in}) = 1 - i\frac{\eta_2^2\bar{\gamma}}{\delta_2} - i\frac{\eta_1^2\bar{\gamma}}{\delta_1 - \frac{a^2}{\delta_2}}\left(1 - \frac{a\eta_2}{\delta_2\eta_1}\right)^2$$

$$\delta_1 = \omega_{in} - \omega_1^b + \frac{i}{2}\left(\alpha_1 + \eta_1^2\bar{\gamma}\right) - \eta_1^2\bar{\Delta}^{rad}$$

$$\delta_2 = \omega_{in} - \omega_2^b + \frac{i}{2}\left(\alpha_2 + \eta_2^2\bar{\gamma}\right) - \eta_2^2\bar{\Delta}^{rad}$$

$$a = i\eta_1\eta_2\left(\frac{\bar{\gamma}}{2} + i\bar{\Delta}^{rad}\right)$$

$$1 = \eta_1^2 + \eta_2^2$$

where t represents the transmission amplitude, ω_{in} the incident frequency, $\omega_{1,2}^b$ the resonant frequencies, $\alpha_{1,2}$ the loss coefficients, $\eta_{1,2}$ the relative coupling weights, $\bar{\gamma}$ the coupling loss coefficients, and $\bar{\Delta}^{rad}$ the reactive radiative coupling coefficient. Notice that $\bar{\Delta}^{rad}$ indicates a net shift of the resonances (Lamb-shift) [36]. By measuring both the spectral transmission and the phase it is possible to fit the two curves by the same set of parameters, thus reducing possible parameter dependencies and verifying the model. Figure 3 shows the experimental transmission and phase for a micro-resonator. In this example, two radial families are coupled and a third radial family is uncoupled. The model considers all these three families, which allows reaching a high agreement between experiment and theory.

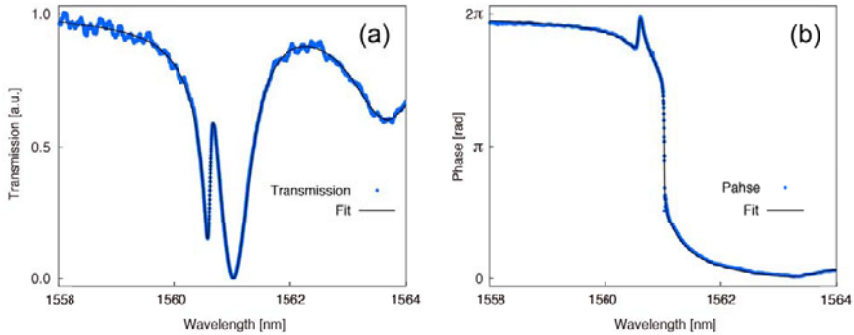

Figure 3. Measured (broad data points) and simulated (narrow line) transmission (a) and phase (b) spectra as a function of the incident wavelength.

The shape of the phase spectrum reveals under- and over-coupling regimes for the narrow and broad coupled resonances. The relevant parameters extracted from the fir are: $\eta_1 = 0.9737 \pm 0.0001$, $\bar{\gamma} = 0.07574 \pm 0.00034$ THz , $\alpha_1 = 0.0205 \pm 0.00034$ THz , $\alpha_2 = 0.00601 \pm 0.000059$ THz and $\bar{\Delta}^{rad} = -0.1135 \pm 0.00015$ THz where η_1 and $\bar{\Delta}^{rad}$ indicates a weak intermodal coupling and a red-shift optical lamb-shift.

Coupling among resonances and chaotic response

Optically induced thermal and free carrier nonlinearities in a silicon microring resonator have been intensely studied. Under continuous wave excitation, a bistable regime is established by the dominant nonlinearity [37]. Optical bistability has paid high interest as the phenomenon that enables the implementation of all-optical switching, logical gates and memories [38, 39]. At a certain input power, other competing non-linear mechanisms could emerge inducing an oscillatory time response [40, 41, 42, 43, 44]. We observed that the addition of several coupled cavities in the optical system could enrich the nonlinear response, from bistable or self-pulsing regimes to a chaotic time response [45]. In particular, the intracavity feedback of optical modes established in a chain of resonators defining a SCISSOR (Side-Coupled Integrated Spaced Sequence of Resonators) configuration could provides the necessary input for the onset of chaotic oscillations.

In fact, the measured aperiodic signal (figure 4a) shows a complete lack of regularities and thus, suggests the presence of chaos. One of the distinguishing features of a chaotic dynamical system is the high sensitivity to the initial conditions (figure 4). Two trajectories, which start from slightly different initial conditions rapidly, lose correlation as the system evolves. The sensitivity to the initial conditions is proven as follows: the input signal of a given wavelength is square wave modulated with a 2% duty cycle. The pump switch-off duration is nearly 1ms, which is sufficient to let the SCISSOR to relax and thermalize with the environment. The experimental noise (chip temperature and pump intensity fluctuations) makes the initial conditions slightly different every square wave edge front. Figure 4a shows that two periodic sequences with small different initial conditions evolve towards two identical signals that are again periodic and

slightly delayed. The case of two aperiodic outputs is different: after few microseconds (~30 μs), the waveforms completely lose their similarity. As shown in figure 4b, the cross correlation between the two aperiodic sequences vanishes, meaning that the small perturbations of the initial state are modifying the evolution of the system [45].
This observation of chaos in a SCISSOR could be relevant for the generation of random data sequences, both in the electrical and in the optical domain within the Si-photonics framework.

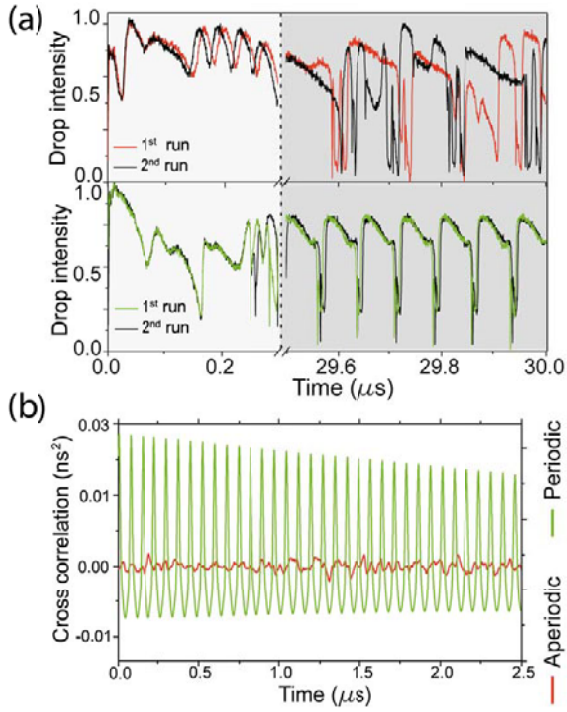

Figure 4. Time evolution (a) and Cross correlation (b) of two periodic (aperiodic) signals, indicated as run 1 and 2, which start from slightly different initial conditions.

Application: Biosensors based on microresonators

The last point of the article treats an application of micro-resonators as the label-free biosensors. The integrated optics-based detection system is one of the most suitable technologies for lab-on-chip applications for real time detection of molecular interactions [46] owing to the possibility of its miniaturization, extreme sensitivity (molecular interactions), robustness, reliability, and its potential for multiplexing.

In the label-free biosensing approach, the target molecule (analyte) is selectively captured on the surface of the micro-resonator by a bio-recognition agent, immobilized on the surface of the sensor. The trapped molecules form a layer that can be directly measured by quantifying the changes in the effective refractive index of the optical mode of a micro-resonator. Since the resonance wavelength depends on the effective refractive index of the mode, a shift in the resonant spectral position is directly linked to a variation in the refractive index, i.e. to the detection of the target molecule [47].

Our device is composed by a multiplexed system of 4 micro-resonators (figure 5): two have the cladding layer removed and are functionalized for a redundant measurement, one has the cladding removed but it is not functionalized to measure the aspecific response and the last is covered by the cladding (i.e. protected by the liquid) for reference.

First we assessed the bulk Sensitivity (S). The spectral shifts of the resonances were monitored in real-time, while the devices were exposed to glucose-water solutions of various concentrations. The refractive index of such solutions can be easily measured or estimated [48, 49, 50]. For n_{SiON}=1.66, the best sensitivity was S=82 nm/RIU (Refractive Index Units) with a very good reproducibility (error in the order of 1%).

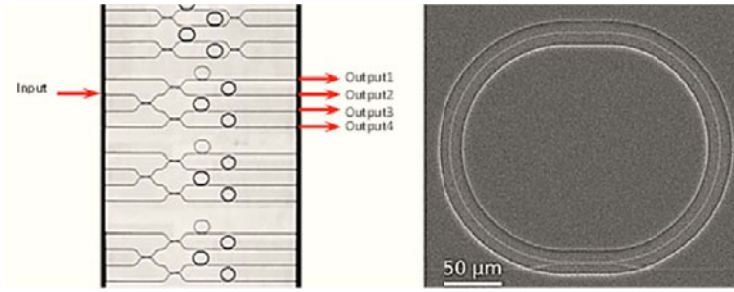

Figure 5. (Left) Top-view microscope image of the 1x4 multiplexed sensor prototype. (Right) SEM image of the opening window around a micro-resonator.

Then, the Limit of Detection (LOD) was measured. The LOD is defined as the minimum input quantity that can be distinguished with more than 99% fidelity, and can be calculated as $LOD = 3\epsilon/S$, where ϵ is the output uncertainty, given as the standard deviation obtained on repeated measurements of a blank solution. From the measurement on three micro-resonators, the same value of $LOD \simeq 3x10^{-6}$ RIU was measured. Finally, we performed sensing measurements [48, 50]. After surface functionalization with DNA-aptamers we flowed a solution where in a

DMSO buffer Aflatoxin M1 toxin was diluted. The lowest concentration of Aflatoxin M1 that we were able to detect was as low as 1.58 nM [50].

CONCLUSIONS

The phase measurements is an interesting tool to distinguish between coupling regimes in the micro-resonator/bus-waveguide optical system. Additionally, the simultaneous fit of several resonances in the vertical coupling scheme represents another tool to study the intermodal coupling mediated by the waveguide, and the optical lamb-shift. The addition of coupled cavities gives rise to a chaotic signals that could be employed to generate random numbers, for i.e. secure data transmissions. The resonator-based biological detection system is a platform for a miniaturized lab-on-a-chip. All of these phenomena/applications have been proved by using Silicon Photonics, a mass-production enabled and CMOS compatible technology.

ACKNOWLEDGMENTS

We acknowledge financial support from the Autonomous Province of Trento, partly under the Call "Grandi Progetti," Project "On Silicon Chip Quantum Optics for Quantum Computing and Secure Communications—SiQuro." I.C. acknowledges partial support by a grant from the European Research Council (ERC, QGBE, 267159). The biosensing activity was performed within the frame of the European project Symphony (Grant number: 610580). The authors would like to thank the MNF Facility of Fondazione Bruno Kessler, Centre for Materials and Microsystems, for device fabrication. We also would like to thank E. Moser for helpful discussions.

REFERENCES

1 J. Chen, Y. Gong, M. Fiorani, and S. Aleksic, *IEEE Commun. Mag.* **53**, 140 (2015).
2 C. Kachris, K. Kanonakis, and I. Tomkos, *IEEE Commun. Mag.* 51, 39 (2013).
3 L. Pavesi and G. Guillot, Optical interconnects, *Springer Series Opti.* **119** (2006).
4 R.-J. Essiambre and R. W. Tkach, *P. IEEE*, **100**, 1035 (2012).
5 Minnesota Internet Traffic Study (MINTS). referenced on: http://www.dtc.umn.edu/mints/
6 G. P. Agrawal, "Nonlinear fiber optics". (Academic Press – 2007).
7 R.-J. Essiambre and R. W. Tkach, *P. IEEE*, **100**, 1035 (2012).
8 C. A. Brackett, IEEE J. Sel. Area Comm. **8**, 948 (1990).
9 G. Moore, Electronics Magazine **38**, 114–117 (1965).
10 J. D. Plummer, "Silicon VLSI technology: fundamentals, practice, and modeling". Pearson (Education – 2009)
11 M. Waldrop, *Nature* **530**, 144 (2016).
12 G. T. Reed and A. P. Knights, "Silicon photonics" (Wiley Online Library – 2008).
13 L. Pavesi and D. J. Lockwood, "Silicon photonics, vol. 1". (Springer Science & Business Media – 2004)
14 D. Dai and J. E. Bowers, *Nanophotonics*, **3**, 283 (2014)

15 The fabrication process of some materials such as III-V semiconductors, for essentially providing light sources an detectors, are not CMOS compatible but are integrated usually as discrete components on the Silicon-based chip.
16 Y. Li, S. Verstuyft, G. Yurtsever, S. Keyvaninia, G. Roelkens, D. Van Thourhout, and R. Baets, *Appl. Optics*, **52**, 2145 (2013).
17 K. De Vos, I. Bartolozzi, E. Schacht, P. Bienstman, and R. Baets, Opt. Express, **15**, 7610 (2007)
18 F. B. Myers and L. P. Lee, *Lab. Chip*, **8**, 2015 (2008)
19 B. Redding, S. F. Liew, R. Sarma, and H. Cao, *Nat. Photonics*, **7**, 746 (2013).
20 N. Jokerst, M. Royal, S. Palit, L. Luan, S. Dhar, and T. Tyler, *J. Biophotonics*, 212 (2009).
21 T. Van Vaerenbergh, M. Fiers, P. Mechet, T. Spuesens, R. Kumar, G. Morthier, B. Schrauwen, J. Dambre, and P. Bienstman, *Opt. Express*, **20**, 20292 (2012).
22 K. Vandoorne, P. Mechet, T. Van Vaerenbergh, M. Fiers, G. Morthier, D. Verstraeten, B. Schrauwen, J. Dambre, and P. Bienstman, *Nature Commun.* **5**, 3541 (2014).
23 F. Ramiro-Manzano, N. Prtljaga, L. Pavesi, G. Pucker and M. Ghulinyan, *Opt. Express*, 20, 22934 (2012).
24 M. Mancinelli, M. Borghi, F. Ramiro-Manzano, J. Fedeli, and L. Pavesi, *Opt. Express*, **22**, 14505 (2014).
25 R. Guider, D. Gandolfi, T. Chalyan, L. Pasquardini, A. Samusenko, G. Pucker, C. Pederzolli, L. Pavesi, *Sensors.* **15**, 17300 (2015).
26 G. C. Righini, Y.Dumeige, P. F_eron, M. Ferrari, G. Nunzi Conti, D. Ristic, and S. Soria. *Riv. Nuovo Cimento*, **34**, 435 (2011).
27 D. G. Rabus. "Integrated Ring Resonators" (Springer,- 2007).
28 A. Yariv. *IEEE Photonic. Tech. L.* **14**, 483, (2002).
29 M.Ghulinyan, R.Guider, G.Pucker, and L.Pavesi *IEEE Photonic. Tech. L*. **23**, 1166 (2011)
30 M. Ghulinyan, F. Ramiro-Manzano, R. Guider, N. Prtljaga, G. Pucker and L. Pavesi, *Proc. SPIE* 8431 (2012).
31 F. Ramiro-Manzano, N. Prtljaga, L. Pavesi, G. Pucker and M. Ghulinyan, *Opt. Letters*, **38**, 3562 (2013).
32 F. Ramiro-Manzano, M. Ghulinyan, N. Prtljaga, G. Pucker, L. Pavesi, Proc. SPIE 8600 (2013)
33 F. Ramiro-Manzano; N. Prtljaga; L. Pavesi; G. Pucker; M. Ghulinyan, *Opt. Express*, **20**, 22934 (2012)
34 M. Ghulinyan, F. Ramiro-Manzano, N. Prtljaga, R. Guider, I. Carusotto, A. Pitanti, G. Pucker; and L. Pavesi, *Phys. Rev. Lett.* **110**, 163901 (2013)
35 To be published
36 M. Ghulinyan, F. Ramiro Manzano, N. Prtljaga, M. Bernard, L. Pavesi, G. Pucker and I. Carusotto, *Phys. Rev. A* **90**, 053811 (2014)
37 V. R. Almeida and M. Lipson, "Optical bistability on a silicon chip," *Opt. Lett.* **29**, 2387 (2004).
38 P. E. Barclay, K. Srinivasan, and O. Painter, *Opt. Express* **13**, 801 (2005).
39 Q. Xu and M. Lipson, *Opt. Express* **15**, 924 (2007)
40 T. J. Johnson, M. Borselli, and O. Painter, *Opt. Express* **14**, 817 (2006).
41 G. Priem, P. Dumon,W. Bogaerts, D. Van Thourhout, G. Morthier, and R. Baets, *Opt.*

Express 13, 9623 (2005)
42 T. Van Vaerenbergh, M. Fiers, P. Mechet, T. Spuesens, R. Kumar, G. Morthier, B. Schrauwen, J. Dambre, and P. Bienstman, *Opt. Express* 20, 20292 (2012).
43 T. Van Vaerenbergh, M. Fiers, P. Mechet, T. Spuesens, R. Kumar, G. Mortier, K. Vandoorne, B. Schneider, B. Schrauwen, J. Dambre, and P. Bienstman, in Asia Communications and Photonics Conference, *J. Opt. Soc. Am.* (2012)
44 T. Van Vaerenbergh, M. Fiers, J. Dambre, and P. Bienstman, *Phys. Rev. A* **86**, 063808 (2012)
45 M. Mancinelli, M. Borghi, F. Ramiro-Manzano, J. M. Fedeli and L. Pavesi, Opt. Express, **22**, 14505 (2012)
46 M.C. Estevez, M. Alvarez, L.M. Lechuga, Laser & Photonics Reviews. **6**, 463 (2012)
47 C. Ciminelli, C.M. Campanella, F. Dell'Olio, C.E. Campanella, M.N. Armenise, *Prog. Quantum Electron.***37**, 51 (2013)
48 A. Samusenko, D. Gandolfi, G. Pucker, T. Chalyan, R. Guider, M. Ghulinyan and L. Pavesi. *J. Lightwave Technol.* **34**, 969 (2016);
49 D. Gandolfi "On-chip photonic label-free biosensors". PhD Thesis, University of Trento, Trento, Italy (2015)
50 T. Chalyan, D. Gandolfi, R. Guider, L. Pavesi, L.Pasaquardini, C. Pederzolli, A. Samusenko, G. Pucker, *IEEE BioPhotonics* (2015)